LATE-STAGE FATIGUE DAMAGE IN A GLASS/EPOXY NON-CRIMP 3D ORTHOGONAL WOVEN FABRIC COMPOSITE

L Baiocchi[a,b], T F Capell[b], S A McDonald[c], S L Ogin[b*], P Potluri[c], M Quaresimin[a], P A Smith[b], P J Withers[c], A Bogdanovich[d]

[a] *Dipartimento di Tecnica e Gestione dei sistemi industriali - Università di Padova, Stradella S.Nicola 3 - 36100 VICENZA, Italy*
[b] *Department of Mechanical Engineering Sciences, Faculty of Engineering and Physical Sciences, University of Surrey, Guildford, UK, GU2 7XH*
[c] *School of Materials, University of Manchester, Manchester, UK, M13 9PL*
[d] *College of Textiles, North Carolina State University, 1000 Main Campus Dr. Raleigh, NC 27695*
** S.Ogin@surrey.ac.uk*

Keywords: damage accumulation, 3D reinforcement, fatigue.

Abstract

Damage development in the later stages of the fatigue life of a glass/epoxy non-crimp 3D orthogonal woven fabric composite has been examined using a combination of mechanical testing and damage observations. Changes in both the stiffness reduction rate and the energy dissipation per cycle suggest that there are three stages in the fatigue lifetime. Observations of damage using X-ray micro computed tomography (CT) and optical microscopy within specimens cycled to the beginning of the third stage show extensive matrix cracking extending between surface weft tows, with associated resin pocket cracking. It is suggested that the observation of extensive fibre fractures within sections of warp tows closest to z-crowns is a consequence of stress concentrations due to these cracks.

1. Introduction

Laminated composite materials based on plies having fibre reinforcement in two dimensions have found ready applications in complex engineering structures. However, with only the polymer holding adjacent plies together, delamination is a common cause of failure. As reviewed in [1], one powerful remedy is using 3D reinforced fabric preforms which have the advantage of incorporating through-thickness (Z-directional) reinforcing yarns that provide, in a controlled fashion, an extraordinary resistance to delamination unmatched by any other fibre-reinforced composite material. Three variations of 3D woven preforms are available at present: orthogonal, angle interlock and layer-to-layer. Of these variations, the orthogonal preforms (where nearly vertical through-thickness yarns pass through the entire preform thickness) generally yield the highest mechanical properties. Important applications have been demonstrated already, and many more are envisioned in the future, for 3D GFRP and CFRP composites in areas such as ballistic and blast protection (e.g. in personnel and vehicle armour shields), marine structures, wind energy (wind turbine spar caps), aircraft structures (from small components to primary load-bearing structures) and in civil engineering (decks, beams, columns). To date, however, there is a limited understanding of the mechanical behavior of this class of composites. Significant progress has been made for quasi-static

loading cases - see, for example, the review in [1] and recent studies [2, 3] - while fatigue studies are fewer in number [e.g. 4, 5].

This paper reports on a preliminary study into the development of fatigue damage leading to final failure in glass/epoxy non-crimp 3D orthogonal woven fabric composites, focusing here on matrix cracking damage (other damage, including observations on macroscopic delaminations and microdelaminations will be reported elsewhere). In particular, a combination of optical microscopy and X-ray micro computed tomography (X-ray μCT) has enabled the role of matrix cracking in the development of macroscopic tow fracture within the 3D structure to be investigated.

2. Experimental methods

The 3-D fabric used was a 3WEAVE® manufactured by 3TEX with an areal density of 2640 $g \cdot m^{-2}$ called "3D-78" [2]. The resin used was a Shell Epikote 828 (Bisphenol-A) epoxy resin with a Shell epicure nadic methyl anhydride (MNA) curing agent and Ancamine K61B accelerator. The structure of the 3-D orthogonal non-crimp woven fabric consisted of three layers of weft tows interlaced by z-tows, and two layers of warp tows. All of the tows were formed from PPG Hybon 2022 E-glass fibres. Panels 300 mm x 300 mm were manufactured using an in-house wet impregnation technique used in many previous studies [e.g. 6]; a combination of glass fibres and resin having very similar values of refractive index, coupled with a very low void content, produces highly transparent specimens. Test coupons were cut parallel to the warp direction with dimensions 200 mm x 8 mm x 2.2 mm; the specimen width of 8 mm was chosen to reduce the ratio of the specimen width to thickness for the sake of better specimen suitability for the X-ray μCT scanning, while retaining a reasonable specimen width. It is recognized that using a specimen width which is close to the fabric unit cell size, in conjunction with the presence of cut tow ends, may significantly reduce the specimen strength and fatigue life.

Quasi-static and fatigue testing were carried out using Instron series 8800 servo-hydraulic test machines, using 40 mm end tabs, so that the gauge length of the specimens was 120 mm. Extensometers with gauge lengths of either 12.5 mm or 96 mm were used. Fatigue testing was carried out at 5 Hz and an R-ratio of R = 0.1. For hysteresis loop capture, data acquisition every 0.002 s gave 100 data points for each loop. After testing, some specimens were investigated for damage using either optical microscopy or X-ray μCT, or a combination of both techniques. For the X-ray μCT analysis, an area with dimensions 8 mm x 8 mm x 2.2 mm was scanned.

3. Results

3.1 Mechanical test results

The total fibre volume fraction of the 3D woven composite was estimated as ~0.47 (using the matrix burn-off technique). For the warp direction, the Young's modulus (about 24 GPa), ultimate tensile strength (about 420 MPa) and the strain to failure (about 2.4%) were found in good agreement with experimental values reported in [2] for a similar fibre volume fraction and fabric construction. A typical stress-strain curve to failure is shown in Figure 1.

The S-N curve for the specimens, showing maximum stress in the fatigue cycle plotted against number of cycles to failure, is shown in Figure 2. In order to investigate the

development of damage during the later stages of fatigue life, specimens with the longest fatigue lives (using the lowest value of the maximum stress in the fatigue cycle, i.e. 175 MPa) were investigated in more detail. Stiffness reduction and energy dissipation changes with cycle number for a specimen which failed after 90,750 cycles is shown in Figure 3. For these tests, the use of a 96 mm extensometer within a 120 mm gauge length of specimen enhanced the possibility of the final failure occurring somewhere within the extensometer gauge length, as occurred in this case.

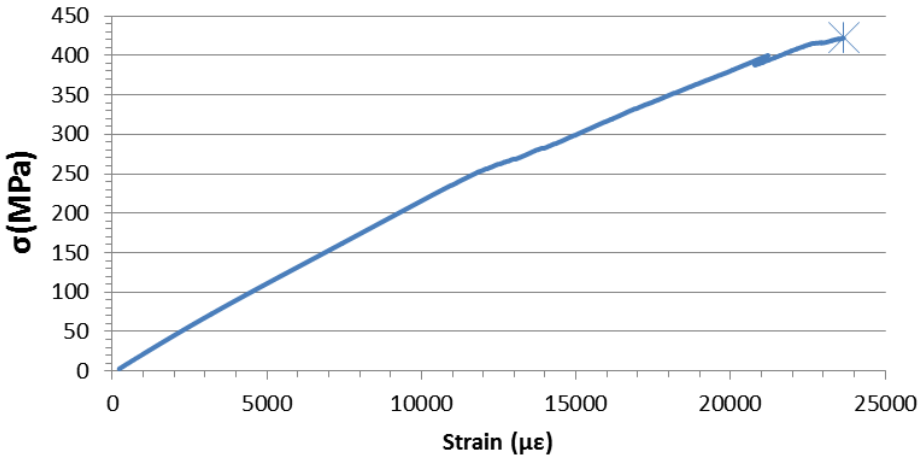

Figure 1. Typical stress-strain curve for a specimen loaded in the warp direction

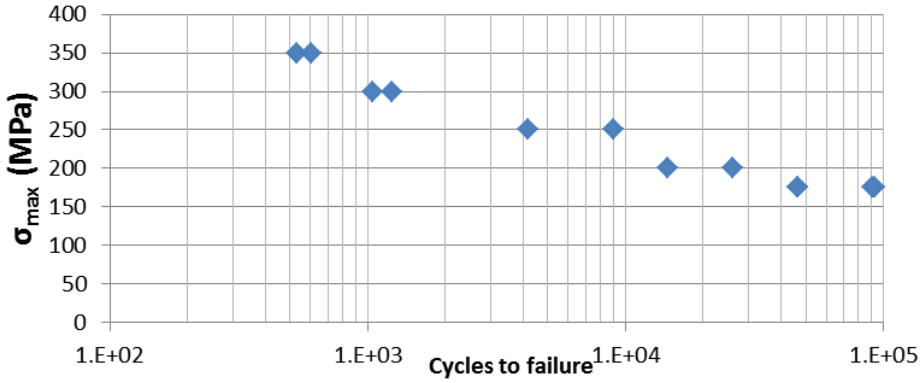

Figure 2. S-N curve for the 3D-78 specimens; gauge length 200 mm x 8 mm x 2.2 mm

The stiffness reduction and energy dissipation show three distinct stages. In the first stage, rapid stiffness reduction, accompanied by high, but rapidly reducing, energy dissipation per cycle, is probably the consequence of rapidly accumulating matrix cracking. The crack density appears to saturate after about 15,000 cycles (for the specimen of Figure 3), leading into the second stage which shows a gradual loss of stiffness accompanied by slowly increasing energy dissipation per cycle. The third stage, leading to specimen ultimate failure, is characterized by a rapidly reducing stiffness accompanied by a large increase in energy dissipation per cycle. The beginning of the third stage was accompanied by audible fibre fractures.

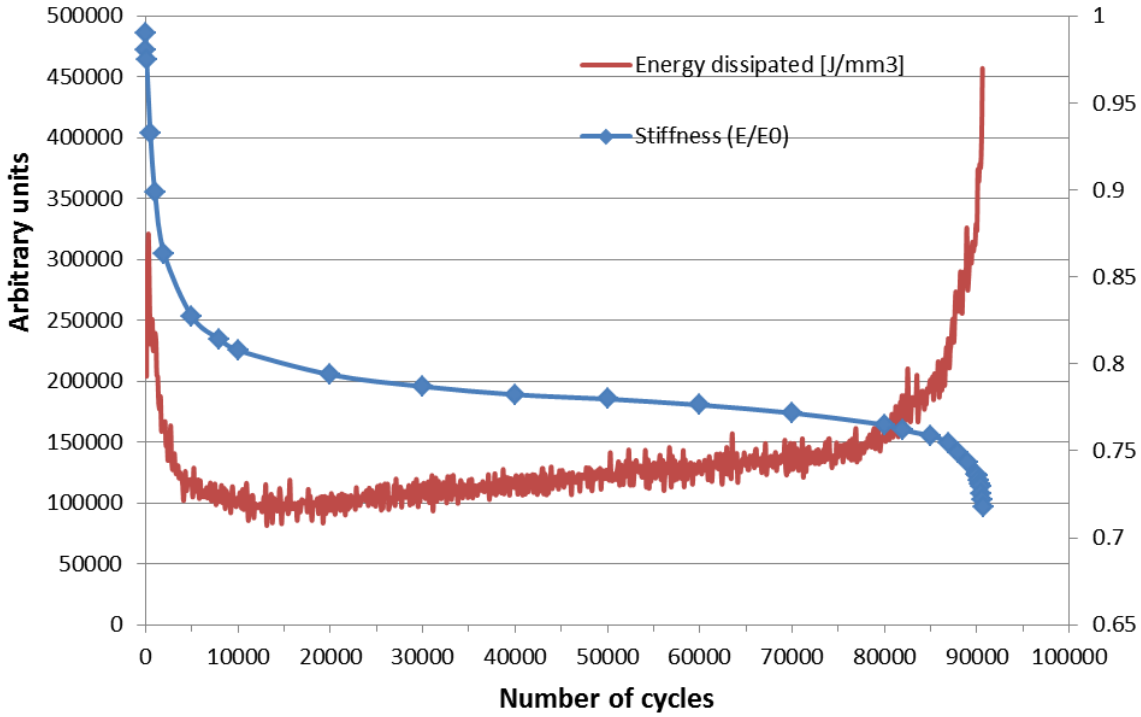

Figure 3. Example of normalized stiffness reduction (right-hand side axis) and energy dissipation (left-hand side axis) with number of cycles for a specimen cycled with a maximum stress of 175 MPa.

3.2 Damage observations

Figure 4 shows a low-magnification image of a specimen which was cycled with a maximum stress of 175 MPa for 46,740 cycles, to the end of the second stage (as the S-N curve shows, Figure 2, the expected number of cycles to failure at this stress level is somewhere between 50,000 and 100,000; the test was interrupted when audible fibre fractures were heard).

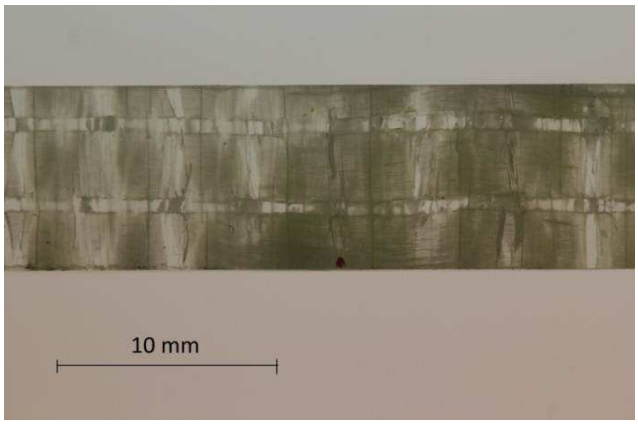

Figure 4. Low magnification image (X-Y plane) of a section of a specimen after 46,740 fatigue cycles

A schematic of the architecture of the 3D-78 specimens is shown in Figure 5, with three vertical through-thickness planes (1, 2 and 3) shown in the vicinity of a z-tow. These planes will be useful in understanding the locations of the planes of the micrographs shown below.

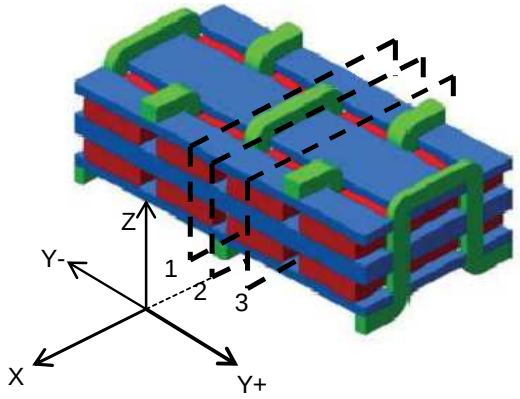

Figure 5. Schematic of the 3D architecture; the X-direction is the loading direction

An X-ray µCT image of the plane labeled as "1" in Figure 5 is shown in Figure 6. Note that the coordinate system shown at the bottom right of Figure 6 is the same as in Figure 5. Hence, with the plane of the z-tow taken as Y = 0, then the plane shown in Figure 6 is Y-negative; it is possible in this image to see the edge of the z-tow, and the end of the z-tow can be seen clearly in the X-Y plane. The significant feature within this image is, however, the presence of extensive fibre fractures in the warp tow; the fractures shown are actually located towards the edge of the warp tow. In addition, the fibre fractures are located, approximately, at the maximum thickness of the surface weft tow, close to where the z-tow crowns over the surface weft tow. Interestingly, no fibre fractures were found within the equivalent section of the lower warp tow of Figure 6. Figure 7 shows another section in the X-Z plane, but 0.5 mm closer to the z-tow. Clustered fibre fractures can again be seen across the thickness of the warp tow, although the fractures are now a little more dispersed.

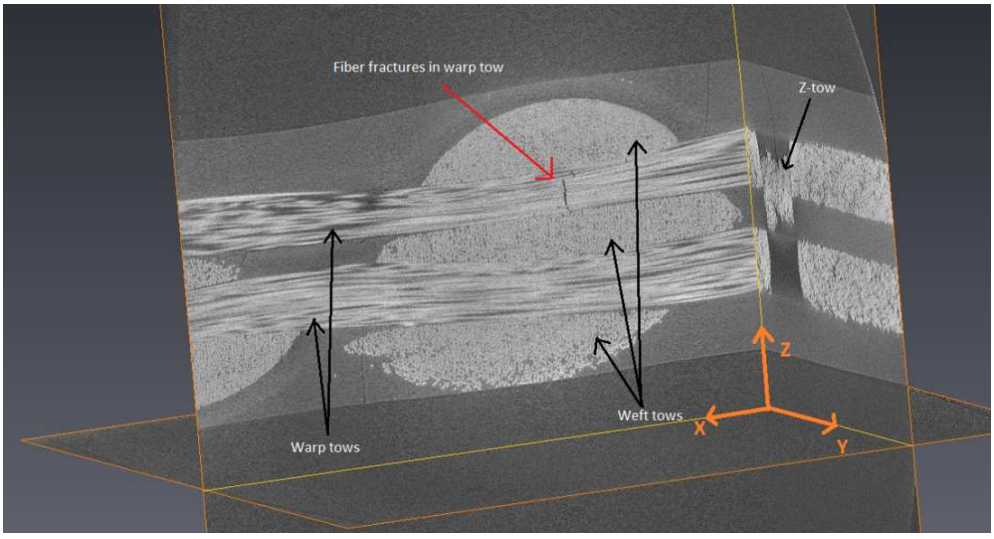

Figure 6. CT section showing extensive fibre fracture towards the edge of a warp tow, located adjacent to the largest thickness of the surface weft tow; note the absence of tow fractures in the lower warp tow.

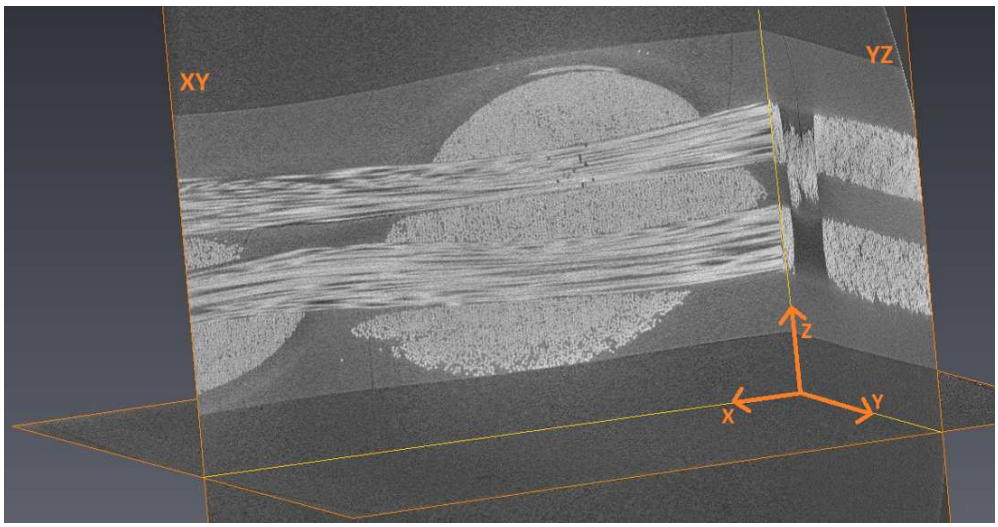

Figure 7. A virtual section at the same X-Z location as Figure 6, but 0.5 mm closer to the plane of the z-tow.

The µCT technique enables virtual slices in orthogonal planes at the same location to be seen. Figure 8 shows a virtual section in the X-Y plane at the same location as the fibre fractures shown in Figures 6 and 7. This image suggests that fibre fractures develop initially at the edges of the warp tows. The figure also shows evidence of matrix cracks within the resin pockets between the two warp tows close to the location of the fibre fractures, though evidence of cracking within the resin pockets is more easily seen in the optical micrographs (see below).

Figure 9 shows two optical micrographs produced after sectioning and polishing the specimen; the plane of Figure 9(a) is almost exactly the same plane as the µCT image of Figure 6 (i.e. Y-negative), and the same cluster of warp tow fibre fractures can be seen. Immediately above the cluster of fibre fractures in the image of Figure 9(a), a matrix crack in the surface weft tow can be seen. Figure 9(b) shows the same X-Z location as Figure 9(a), but at position Y = 0 i.e. the plane of the z-tow (which is the plane labelled "2" in Figure 5). In this plane, the warp tows cannot be seen and the gap between the weft tows is filled by resin pockets. It is evident that the matrix crack in the resin pocket is an extension of the matrix crack in the surface weft tow. Indeed, the same matrix crack appears to extend from the resin pocket through the middle weft tow, through the second resin pocket, and through the surface weft tow adjacent to the opposite surface. Such combined X-ray µCT/optical micrograph observations of matrix cracking and tow fractures were confirmed in a second specimen.

These observations suggest that the cluster of fibre fractures at the edge of the warp tows are the consequence of stress concentrations caused by cracks which extend around the circumference of the warp tows near the edge of the tows (matrix cracks in the weft tows and extensions of these cracks in the resin pockets). The absence of fibre fractures in the lower warp tow, at D in Figure 9(a), may be a consequence of the micro-delamination which has formed from the matrix crack at this location; this would reduce the stress concentration due to the matrix crack in this surface weft tow.

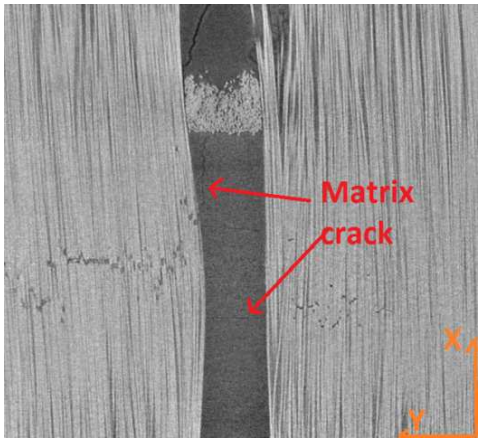

Figure 8. Evidence of matrix cracking in Y-Z plane within the resin pocket between two warp tows adjacent to fibre fractures.

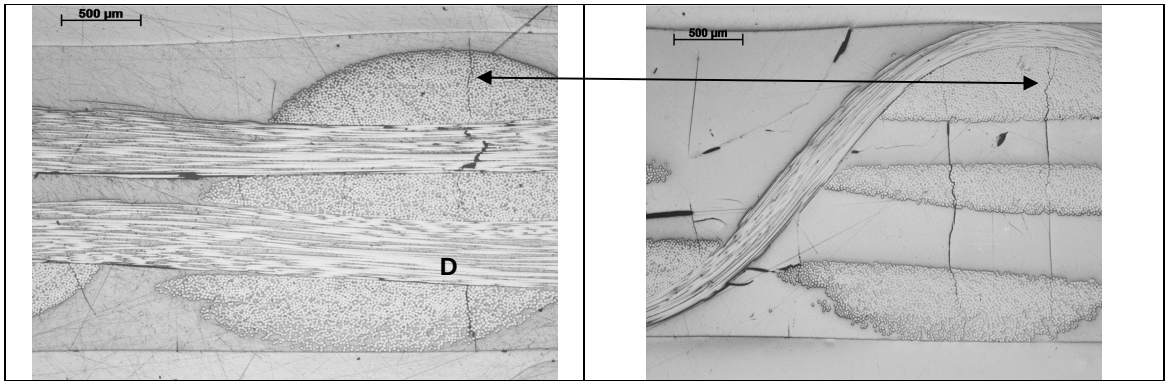

(a) (b)

Figure 9. (a) Optical micrograph of sectioned and polished specimen showing the same tow fracture as seen in Figure 6 (i.e. the X-Z plane). (b) Optical micrograph at the same X-Z location but for the plane Y = 0 (i.e. the plane of the z-tow). The arrow indicates the matrix crack in the surface weft tow which continues through the resin pocket that is located between the warp tows (the warp tows cannot be seen in this cross-section).

4. Concluding remarks

This preliminary study of late-stage fatigue damage in a glass/epoxy non-crimp 3D orthogonal woven fabric composite has suggested, as a general outcome, that there is considerable value in combining X-ray micro computed tomography with optical microscopy when investigating damage in composite materials with complex architectures.

Measurements of stiffness reduction and energy dissipation suggest that there are three major stages in the development of damage within these composites. In general terms, these stages are similar to the damage development stages found in many other composite materials. The first stage, characterized by a rapid loss of stiffness and high energy dissipation per cycle, leads into a second stage where the stiffness reduction rate and energy dissipation is lowest. The transition to the third stage sees an increased stiffness reduction rate and rapid rise in energy dissipation per cycle up to failure. For this investigation, specimens were cycled to the point of transition between the second and third stages. The observations have shown that at

this point in the fatigue life of the 3D-78 specimens, clusters of fibre fractures develop at the edge of warp tows which are closet to z-crowns. These fibre fractures may be the consequence of matrix cracks which extend fully across the composite between the surface weft tows; these cracks also extend, in the same plane, into the resin pockets between the warp tows. The consequence is that a fibre located at the edge of a warp tow experiences, from one direction, a stress concentration due to a matrix crack in an adjacent weft tow, and from an orthogonal direction, a stress concentration due to the extension of the weft tow matrix crack into the resin pocket. Such stress concentrations in sections of warp tows away from z-crowns are likely to be reduced by the development of micro-delaminations.

One important structural feature of the studied 3D woven composite is the absence of interlacing between warp and weft tows which results in their practical straightness; this feature distinguishes them from many other textile composites, like 2D weaves, 2D and 3D braids, 3D interlock weaves, weft knits, etc. The other important structural feature is the presence of z-tows which are interlaced with adjacent weft tows, but only at the fabric facings. These two features bring many new peculiarities into the damage initiation and propagation processes, particularly observed under fatigue loading. Some of these consequences are clearly seen in the results of this paper. Further work is required to understand fully the sequence of damage development at all stages of the fatigue life and, specifically, the development of micro-delaminations which seem associated with surface weft tows that do not have z-crowns.

Acknowledgements

We are grateful to the Engineering and Physical Sciences Research Council (EPSRC) grants EP/F007906/1 and EP/F028431/1 for funding the Henry Moseley X-ray imaging facility.

References

[1] A. E. Bogdanovich and M. H. Mohamed. “Three-dimensional reinforcements for composites.” SAMPE Journal, vol 45, 2-20, 2009

[2] S. V. Lomov, A. E. Bogdanovich, D. S. Ivanov, D. D. Mungalov, M. Karahan and I. Verpoest. “A comparative study of tensile properties of non-crimp 3D orthogonal weave and multi-layer plain weave E-glass composites. Part 1: Materials, methods and principle results.” Composites: Part A, vol 40, 1134-1143, 2009.

[3] A. E. Bogdanovich, M. Karahan, S. V. Lomov and I. Verpoest. “Quasi-static tensile behavior and damage of carbon/epoxy composite reinforced with 3D non-crimp orthogonal woven fabric.” Mechanics of Materials, vol 62, 14-31, 2013.

[4] V. Carvelli V, G. Gramellini , S. V. Lomov, A. E. Bogdanovich, D. D. Mungalov and I. Verpoest I (2010) “Fatigue behaviour of non-crimp 3D orthogonal weave and multi-layer plain weave E-glass reinforced composites.” Composites Science and Technology, vol 70, 2068-2076, 2010.

[5] A. P. Mouritz. “Tensile fatigue of properties of 3D composites with through-thickness reinforcement.” Composites Science and Technology, vol 68, 2503-2510, 2008.

[6] H. M. S. Belmonte, C. I. C. Manger, S. L. Ogin, P.A. Smith, R. Lewin. “Characterisation and modelling of the notched tensile fracture of woven quasi-isotropic GFRP laminates.” Composites Science and Technology, vol 61, 585-587, 2001